Magn Reson Mater Phy (2009) 22:151–158
DOI 10.1007/s10334-008-0159-6

RESEARCH ARTICLE

How background noise shifts eigenvectors and increases eigenvalues in DTI

Frederik Bernd Laun · Lothar Rudi Schad · Jan Klein · Bram Stieltjes

Received: 1 July 2008 / Revised: 18 November 2008 / Accepted: 18 November 2008 / Published online: 9 December 2008

Abstract
Indroduction The signal-to-noise ratio of in vivo diffusion tensor imaging (DTI) is usually very limited, especially if high resolution data is acquired. In a variety of settings, the signal of diffusion weighted images can drop below the background noise level yielding an underestimated diffusion constant. In this work, we report two new artefacts in DTI that are important in this regime.
Methods Both artifacts are described analytically and numerically and are demonstrated in DTI phantoms and in subjects in vivo.
Results First, eigenvectors are systematically shifted towards distinct 'attractive' orientations of the gradient scheme. Second, certain eigenvalues can be overestimated due to the underestimation of the measured diffusion, which can result in the misordering of eigenvalues
Discussion We show that these effects are relevant for current clinical settings of DTI.

Keywords Diffusion tensor imaging · Eigenvector shift · Background noise · Eigenvalues · Overestimation · Artefacts · High *b* value

F. B. Laun (✉) · B. Stieltjes
Medical Physics in Radiology, German Cancer Research Center, Heidelberg, Germany
e-mail: f.laun@dkfz.de

L. R. Schad
Lehrstuhl für Computerunterstützte Klinische Medizin, Medizinische Fakultät Mannheim, Universität Heidelberg, Mannheim, Germany

J. Klein
MeVis Research, Bremen, Germany

Introduction

Typically, the signal-to-noise ratio (SNR) of in vivo diffusion weighted images is small and image averaging is needed to enable a stable calculation of the diffusion tensor and derived values like fractional anisotropy (FA) and apparent diffusion coefficient (ADC, the third of the trace of the diffusion tensor). Magnitude images are commonly used for averaging since phase instabilities induced by the diffusion sensitizing gradients hamper complex averaging. Magnitude averaging reduces the uncertainty but does not prevent that the signal is biased at low SNR [1,2]. This becomes increasingly prominent at high resolutions, high *b* values or pathological high ADCs. In these cases, the signal may already be reduced below the background noise level, since it decays rapidly if the diffusion weighting is applied along a principal axis of the diffusion tensor. Jones et al. showed that this causes an *underestimation* of diffusion, FA and ADC [3].

Considering the precision of DTI, several authors pointed out the importance of the gradient scheme. The gradient scheme determines the uncertainty of measurements in an tensor orientation dependent fashion [4–7]. Andersson [8], Koay [9–12] and Chang [13] presented powerful frameworks to describe the propagation of error from the measured signals to the diffusion tensor and to derived values like FA. Besides the precision, Jones et al. [14] recognized that the mean values of FA and ADC are also dependent on the spatial orientation of the diffusion tensor towards the gradient scheme for low signal to noise ratios (SNR) in diffusion weighted images [14].

In this work, two new artefacts which are important in this regime and which are related to the employed gradient scheme are presented. They are relevant in high resolution and high *b* value measurements. We show both, in computations and in phantom measurements that certain eigenvalues can be *overestimated* due to the underestimation of the diffusion [3] and that eigenvectors are shifted from their true orientation in a systematic fashion.

Theory

The paper addresses noise effects in DTI that result from low SNR in diffusion weighted images, where the condition

$$S_0 \exp\left(-b\vec{g}_i^T D\vec{g}_i\right) > \sigma \tag{1}$$

is violated. Here, S_0 is the signal without diffusion weighting, σ is the standard deviation of the complex signal [2], b (or b value) is the strength of the diffusion weighting, $\vec{g}_i = \left(g_{ix}, g_{iy}, g_{iz}\right)^T$ is a unit vector pointing along the diffusion gradient direction and D is the symmetric diffusion tensor

$$D = \begin{pmatrix} D_{xx} & D_{xy} & D_{xz} \\ D_{xy} & D_{yy} & D_{yz} \\ D_{xz} & D_{yz} & D_{zz} \end{pmatrix} \tag{2}$$

which has six independent elements. We assume that a log-linear tensor estimation is employed [4]. Then, D is determined by measuring tensor projections

$$p_i = \vec{g}_i^T D\vec{g}_i = -\ln(S_i/S_0)/b \tag{3}$$

along N directions $\vec{g}_i^T$. The signal S_i is the diffusion-weighted signal. At least six non-colinear directions $\vec{g}_i^T$ must be used for the determination of the six independent elements of D. When using a log-linear tensor estimation [4], the tensor elements are reordered in a vector $\vec{d} = \left(D_{xx}, D_{yy}, D_{zz}, D_{xy}, D_{xz}, D_{yz}\right)^T$, that is related to the projections $\vec{p} = (p_1, p_2, \ldots, p_N)^T$ by

$$\vec{p} = A\vec{d} \quad \text{and} \quad \vec{d} = A^{-1}\vec{p}, \tag{4}$$

with the transformation matrix A for N gradient directions

$$A = \begin{pmatrix} g_{1x}^2 & g_{1y}^2 & g_{1z}^2 & 2g_{1x}g_{1y} & 2g_{1x}g_{1z} & 2g_{1y}g_{1z} \\ \cdots & \cdots & \cdots & \cdots & \cdots & \cdots \\ g_{Nx}^2 & g_{Ny}^2 & g_{Nz}^2 & 2g_{Nx}g_{Ny} & 2g_{Nx}g_{Nz} & 2g_{Ny}g_{Nz} \end{pmatrix} \tag{5}$$

and A^{-1} being the inverse or pseudoinverse of A.

Overestimation of eigenvalues

In this section, it is shown that certain eigenvalues can be overestimated due to the underestimation of the tensor projections $p_i = \vec{g}_i^T D\vec{g}_i$. The matrix A^{-1} has positive and negative matrix elements. Thus, if the projections p_i are underestimated, elements of $\vec{d}$ and hence the eigenvalues λ_i may be overestimated by 'inappropriate' summation of the p_i. In the following, this is exemplarily shown for the special case of a cigar-shaped tensor with eigenvalues $\lambda_1 > \lambda_2 = \lambda_3$, that is aligned along $(1, 1, 0)^T$ and that is measured with the dual gradient scheme $\vec{g}_i = \{\frac{1}{\sqrt{2}}(1, \pm 1, 0)^T, \frac{1}{\sqrt{2}}(1, 0, \pm 1)^T, \frac{1}{\sqrt{2}}(0, 1, \pm 1)^T\}$.

The tensor in this orientation is

$$D = \frac{1}{2}\begin{pmatrix} \lambda_1 + \lambda_2 & \lambda_1 - \lambda_2 & 0 \\ \lambda_1 - \lambda_2 & \lambda_1 + \lambda_2 & 0 \\ 0 & 0 & 2\lambda_3 \end{pmatrix} \tag{6}$$

and the inverse of transformation matrix is given by

$$A^{-1} = \frac{1}{2}\begin{pmatrix} 1 & 1 & 1 & 1 & -1 & -1 \\ 1 & 1 & -1 & -1 & 1 & 1 \\ -1 & -1 & 1 & 1 & 1 & 1 \\ 1 & -1 & 0 & 0 & 0 & 0 \\ 0 & 0 & 1 & -1 & 0 & 0 \\ 0 & 0 & 0 & 0 & 1 & -1 \end{pmatrix}. \tag{7}$$

The projections are $\vec{p} = (p_1, p_2, p_3, p_3, p_3, p_3)^T$, with $p_1 = \lambda_1$, $p_2 = \lambda_2$, and $p_3 = (\lambda_1 + \lambda_2 + 2\lambda_3)/4$. In the following, the noisy, biased values are denoted by a dash. In the presence of background noise, when condition (1) is violated, the measured projections $p_i' = -\ln(S_i'/S_0')/b$ are smaller than p_i such that $p_i' < p_i$. Moreover, $|p_1' - p_1| < |p_3' - p_3|$ since the signal decays faster along the principal eigenvector and $|p_3' - p_3| \approx |p_2' - p_2|$. With (6) and (7), D_{zz}' can be calculated to be $D_{zz}' = -1 \cdot p_1' - 1 \cdot p_2' + 4 \cdot 1 \cdot p_3' > -p_1 - p_2 + 4p_3 = D_{zz}$. Since the diffusion tensor is aligned along a symmetry axis of the gradient scheme, the eigenvectors cannot shift and there is no mixing between of the x–y plane elements of D' and D_{zz}'. Therefore, D_{zz}' is equal to λ_3'. As a result, the eigenvalue λ_3' increases when p_1' decreases due to the background noise.

For the quantification of this effect the noisy signal can be estimated by

$$S_i' = \sqrt{S_i^2 + \sigma^2}. \tag{8}$$

An exact calculation yields

$$\begin{aligned} \lambda_3' &= -p_1' - p_2' + 4p_3' \\ &= \frac{1}{2b}\left\{\ln\left(\frac{\sqrt{S_0^2 e^{-2b\lambda_1} + \sigma^2}}{S_0'}\right) + \ln\left(\frac{\sqrt{S_0^2 e^{-2b\lambda_2} + \sigma^2}}{S_0'}\right)\right. \\ &\qquad \left. -4\ln\left(\frac{\sqrt{S_0^2 e^{-b(\lambda_1 + 3\lambda_2)/2} + \sigma^2}}{S_0'}\right)\right\} \end{aligned} \tag{9}$$

and

$$\lambda_1' = -\frac{1}{b}\ln\left(\frac{\sqrt{S_0^2 e^{-2b\lambda_1} + \sigma^2}}{S_0'}\right). \tag{10}$$

Hence, the b value at which λ_3' exceeds λ_1' can be estimated. For instance, for an SNR of 10 and $\lambda_1 = 2\ \mu\text{m}^2/\text{ms}$ and $\lambda_2 = \lambda_3 = 0.5\ \mu\text{m}^2/\text{ms}$, λ_3' exceeds λ_1' at $b = 3,000\ \text{s/mm}^2$.

Eigenvector shift

In this section, an example for a systematic eigenvector shift is computed. Consider a cigar-shaped diffusion tensor rotated by an angle θ around the z axis

$$D = \begin{pmatrix} \lambda_1 & 0 & 0 \\ 0 & \lambda_2 & 0 \\ 0 & 0 & \lambda_2 \end{pmatrix} \xrightarrow{Rotation(\theta)} \begin{pmatrix} \lambda_1 \cos(\theta)^2 + \lambda_2 \sin(\theta)^2 & (\lambda_1 - \lambda_2)\sin(\theta)\cos(\theta) & 0 \\ (\lambda_1 - \lambda_2)\sin(\theta)\cos(\theta) & \lambda_2 \cos(\theta)^2 + \lambda_1 \sin(\theta)^2 & 0 \\ 0 & 0 & \lambda_2 \end{pmatrix}. \quad (11)$$

The measured angle θ' can be determined by

$$\theta' = -\frac{1}{2}\arctan\left(2D'_{xy}/\left(D'_{yy} - D'_{xx}\right)\right) \quad (12)$$

Using Eq. (8), the analytical result is given by

$$\theta' = -\frac{1}{2}\arctan \times \left(\frac{\log\left(\frac{\sigma^2 + S_0^2 \exp(-b(\lambda_1+\lambda_2+(\lambda_1-\lambda_2)\sin(2\theta)))}{\sigma^2 + S_0^2 \exp(-b(\lambda_1+\lambda_2-(\lambda_1-\lambda_2)\sin(2\theta)))}\right)}{2\log\left(\frac{\sigma^2 + S_0^2 \exp\left(-b\left(\lambda_2+\lambda_2\cos(\theta)^2+\lambda_1\sin(\theta)^2\right)\right)}{\sigma^2 + S_0^2 \exp\left(-b\left(\lambda_2+\lambda_1\cos(\theta)^2+\lambda_2\sin(\theta)^2\right)\right)}\right)} \right). \quad (13)$$

In Fig. 1, the angular shift $\theta' - \theta$ is plotted versus θ for ADC $= 0.80\ \mu\text{m}^2/\text{ms}$ and FA $= 0.82$. The shift is largest for $\theta = \pm 26°$. It is zero for $\theta = 0°$ and $\pm 45°$ since these orientations correspond to symmetry axes of the gradient scheme. The orientation $\theta = 0°$ is "attractive" since the angular shift $\theta' - \theta < 0$ for small positive θ. For SNR = 19 and $b = 1,000\ \text{s/mm}^2$, the maximal shift is 0.25°. For smaller SNR or larger b values, the angular shift increases ($\theta' - \theta < 1.5°$ for SNR = 7 and $b = 1,000\ \text{s/mm}^2$; $\theta' - \theta < 3.2°$ for SNR = 19 and $b = 2,000\ \text{s/mm}^2$).

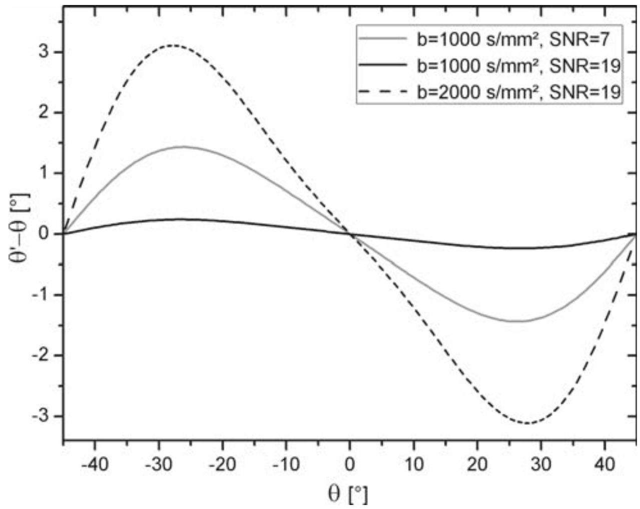

Fig. 1 Theoretically computed angular shift $\theta' - \theta$ for different tensor orientations. θ is the angle that that a cigar-shaped diffusion tensor, which was initially oriented along the x axis, was rotated around the z axis. θ' is the angle determined in the presence of background noise. Computation parameters were ADC $= 0.80\ \mu\text{m}^2/\text{ms}$ and FA $= 0.82$. The angular shift is orientation dependent and maximal for $\theta = \pm 26°$, it becomes increasingly prominent at large b values and small signal-to-noise ratios

Methods

Phantom measurements

A circular DTI-phantom was constructed by winding polyamide fibers (polyfil, consisting of 15 μm fibers, 50 dtex, Filamentgarn TYPE 611, Trevira GmbH, Bobingen, Germany) around an acrylic glass spindle. An aqueous sodium chloride solution (83 g NaCl per kg water) was used as fluid. The concentration of sodium chloride was adapted to match the susceptibility of fibers and fluid [15,16].

The diffusion tensor of the phantom was measured on a Magnetom Avanto 1.5 T scanner (Siemens Medical Solutions, Erlangen, Germany) with a single channel coil, using a spin echo echoplanar sequence. Imaging parameters were TE = 100 ms, TR = 3 s, 10 averages, FOV = $256 \times 72\ \text{mm}^2$, voxel size = $2 \times 2 \times 5\ \text{mm}^3$, partial fourier (6/8), $b = 0$ to $5,000\ \text{s/mm}^2$ in steps of $200\ \text{s/mm}^2$, bandwidth = 2,298 Hz/Px, 6 direction gradient scheme $\{(1, \pm 1, 0)^T, (1, 0, \pm 1)^T, (0, 1, \pm 1)^T\}$.

In vivo measurements

In vivo diffusion-weighted images of the healthy brain were acquired with two parameters sets.

(i) *Clinical setting.* TE = 100 ms, TR = 3 s, 10 averages, FOV = $256 \times 256\ \text{mm}^2$, voxel size = $2 \times 2 \times 2\ \text{mm}^3$, partial fourier (5/8), bandwidth = 2,300 Hz/Px, $b = 0, 1,000\ \text{s/mm}^2$, 6 direction gradient scheme which is rotated around the head-feed axis in steps of 10°, 3 T (Magnetom Trio, Siemens Medical Solutions, Erlangen, Germany), one channel head coil.

(ii) *Very high b value.* TE = 140 ms, TR = 3 s, 3 averages, FOV = $200 \times 200\ \text{mm}^2$, voxel size = $2 \times 2 \times 2\ \text{mm}^3$, partial fourier (6/8), bandwidth = 754 Hz/Px, $b = 0, 8,000\ \text{s/mm}^2$, 6 direction gradient scheme which is rotated around the anterior–posterior axis in steps of 45°, 1.5 T, Grappa with reduction factor two. Here, a 12-channel head coil was employed to improve image quality. Note that the described artefacts are qualitatively observable here, although Ricianity of the Signal is not necessarily conserved.

The acquired images were evaluated in Matlab (The Mathworks, Natick, MA, USA) and NeuroQLab (MeVis Research, Bremen, Germany). Informed consent was obtained from all subjects in accordance with the Declaration of Helsinki, and ethical approval was granted by the ethics committee of the Heidelberg University.

Numerical computations

Numerical computations were performed as follows:

(i) The true diffusion tensor was computed using the free parameters FA and ADC and was rotated into the desired orientation. Cigar shaped tensors were employed.
(ii) The signal was computed for each gradient directions by $S_0 \exp(-b\vec{g}_i^T D \vec{g}_i)$. The 6-directions gradient scheme $\{(1, \pm 1, 0)^T, (1, 0, \pm 1)^T, (0, 1, \pm 1)^T\}$, the 12-directions scheme $\{(1, \pm 0.5, 0)^T, (1, 0, \pm 0.5)^T, (\pm 0.5, 1, 0)^T, \ldots\}$ and the 20- and 30-directions schemes proposed in [4,17] were employed.
(iii) The noisy signal S' was computed numerically assuming a Rician distributed magnitude signal [2]. For SNR larger than 5, these signal expectation values were approximated by Eq. (8), for smaller SNR, they were computed explicitly from the Rician distribution.
(iv) The noisy tensor was estimated with a log-linear model as described in the theory section (Eqs. (3)–(5)) and the corresponding eigenvalues and eigenvectors were computed from the diffusion tensor.

Results

Overestimation of eigenvalues

In Fig. 2a, the measured eigenvalues of the DTI phantom are plotted with respect to the b value using the 6 direction gradient scheme. The eigenvalues were evaluated in two ROIs (Fig. 2b) and are represented by dots. The SNR of the measurement was 19. The FA/ADC values of the phantom (FA $= 0.82 \pm 0.02$, ADC $= 0.80 \pm 0.02$ μm^2/ms), that were used for theoretical calculations (solid lines), were determined at $b = 1{,}000$ s/mm^2, such that the background noise did not influence the measurement.

For b values larger than 1,000 s/mm^2, the measured eigenvalues depend on the applied b value and on the fiber orientation. Eigenvalues in ROI 1 show the 'squashed peanut' behaviour [3]: the second and tertiary eigenvalue remain constant while the principal eigenvalue decreases for b values larger than 1,500 s/mm^2. In ROI 2, the principal eigenvalue decreases at smaller b values ($b = 1{,}000$ s/mm^2) since the fibers are aligned parallel to one of the diffusion directions and hence the signal decays faster. The secondary eigenvalue λ_2 increases non-intuitively for b values larger than 1,250 s/mm^2 and exceeds the primary eigenvalue at $b = 3{,}500$ s/mm^2 which leads to an eigenvalue misordering. This misordering can also be observed on the colormaps of Fig. 2b which were acquired with $b = 1{,}000$ s/mm^2 and $b = 5{,}000$ s/mm^2. The colors represent the principal eigenvector direction. In the $b = 1{,}000$ s/mm^2 measurement, the fiber orientation is represented correctly. But in ROI 2 of the $b = 5{,}000$ s/mm^2 measurement, the principal eigenvector points perpendicular to the fibers which is caused by the misordering of the eigenvalues.

Eigenvector shift

Figure 3 shows the principle eigenvectors of the DTI phantom, that were measured with the b values 1,000 s/mm^2 and 5,000 s/mm^2 using the six direction gradient scheme. The eigenvectors measured with $b = 1{,}000$ s/mm^2 correspond well to the fiber orientation. In the $b = 5{,}000$ s/mm^2 measurement, the eigenvectors in regions corresponding to ROI 1 of Fig. 2b are shifted towards the 'attractive' orientations 'left-right' and 'top-bottom'. Eigenvectors which correspond to ROI 2 of Fig. 2b point perpendicular to the phantom plane. Here, the secondary eigenvector is misinterpreted as the principal eigenvector.

In Fig. 4a–c, the theoretically calculated eigenvector shift for a tensor with FA $= 0.7$ and ADC $= 1$ μm^2/ms is visualized by arrows. The arrows point from the true position of the principal eigenvector to the shifted position on a unit sphere (only a quarter of the sphere is plotted). For six diffusion directions, the eigenvectors are systematically shifted away from the gradient directions towards 'attractive' symmetry axes of the gradient scheme (e.g. towards $(1, 0, 0)^T$). The shift is largest between attractive orientation and diffusion gradient. The shift is zero for eigenvectors pointing along one of the diffusion gradients. For twelve directions, the eigenvector shift is clearly reduced but still present. The pattern of the shift is very similar to that of six directions and the diffusion gradient directions are not necessarily 'distractive' orientations. Figure 4d shows the maximal angular shift of the principal eigenvector for SNR $= 10$. Employing more gradient directions clearly reduces the angular shift, e.g. using 20 gradient directions, the shift is only 0.12° at $b = 1{,}000$ s/mm^2, which is acceptable. Thus, using at least 20 gradient directions mainly eliminates the angular shift of the principal eigenvector.

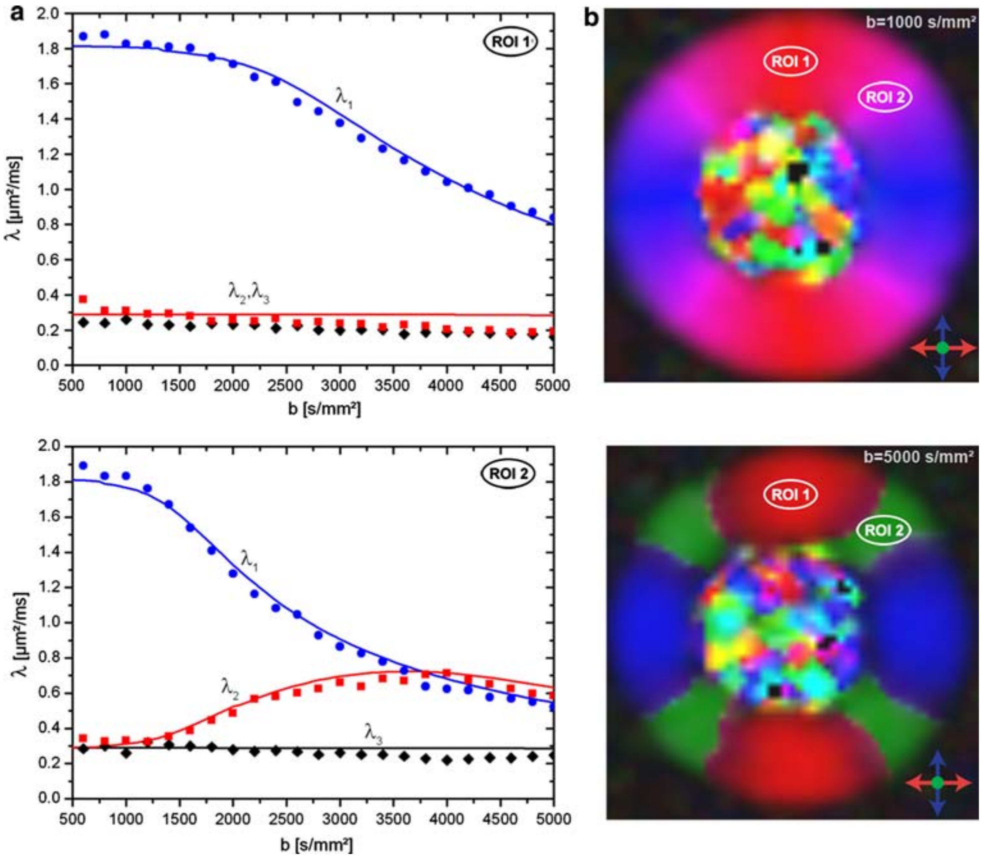

Fig. 2 **a** Eigenvalues of the DTI phantom versus b value for two tensor orientations. **b** Colormap of the circular DTI phantom for $b = 1{,}000$ s/mm^2 and $b = 5{,}000$ s/mm^2. In ROI 2, the secondary eigenvalue λ_2 increases non-intuitively for b values larger than 1,250 s/mm^2 and exceeds the primary eigenvalue at $b = 3{,}500$ s/mm^2 which leads to an eigenvalue misordering. This increase of the secondary eigenvalue is due to the summation procedure of underestimated diffusion values which is employed to calculate the diffusion tensor elements

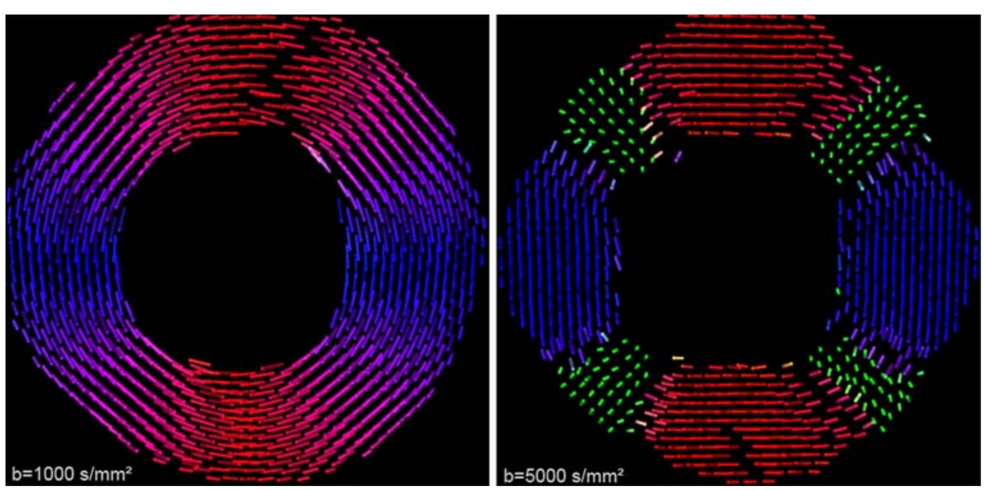

Fig. 3 Principle eigenvectors of the DTI phantom measured with b values 1,000 s/mm^2 and 5,000 s/mm^2. The eigenvectors measured with b = 1,000 s/mm^2 correspond well to the fiber orientation. For b = 5,000 s/mm^2, eigenvectors corresponding to ROI 1 of Fig. 2b are shifted towards the 'attractive' orientations *left-right* and *top-bottom*

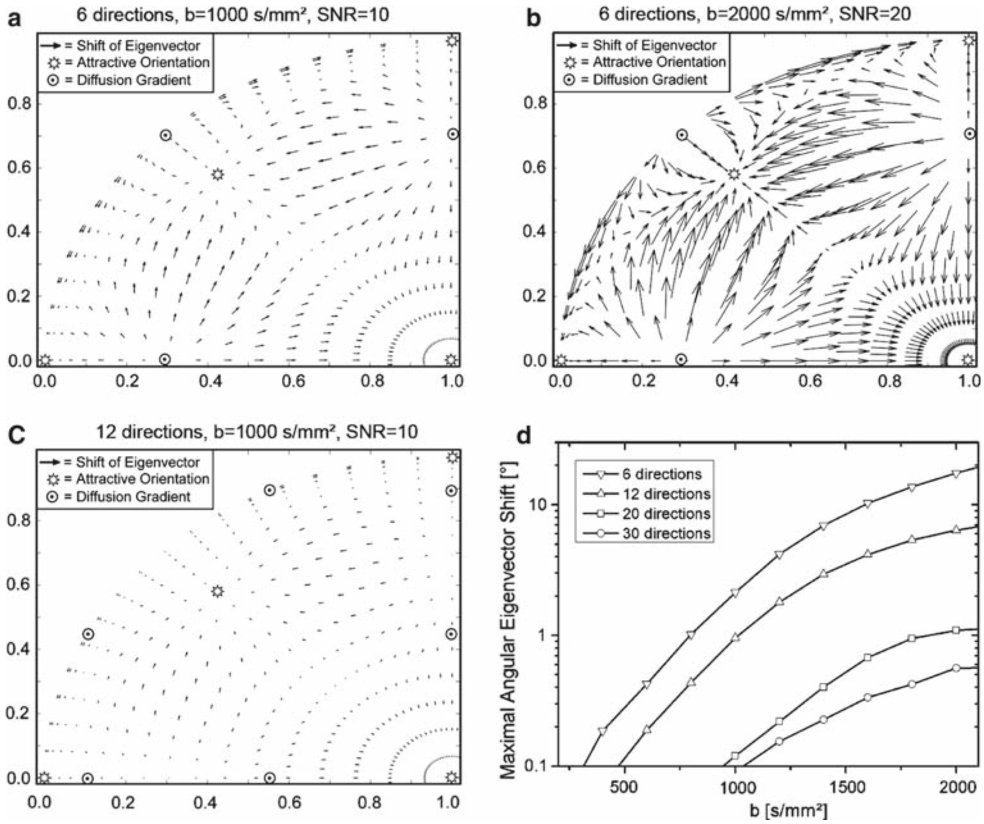

Fig. 4 **a**–**c** Numerically calculated eigenvector shift. Arrows point from the true eigenvector position to the shifted position on a unit sphere. The eigenvectors are systematically shifted away from the gradient directions towards 'attractive' symmetry axes of the gradient scheme (e.g. towards $(1, 0, 0)^T$). For 12 directions, the eigenvector shift is clearly reduced but still present. **d** Maximal angular eigenvector shift in dependency of the b value for SNR = 10. The angular shift is clearly reduced when using more gradient directions

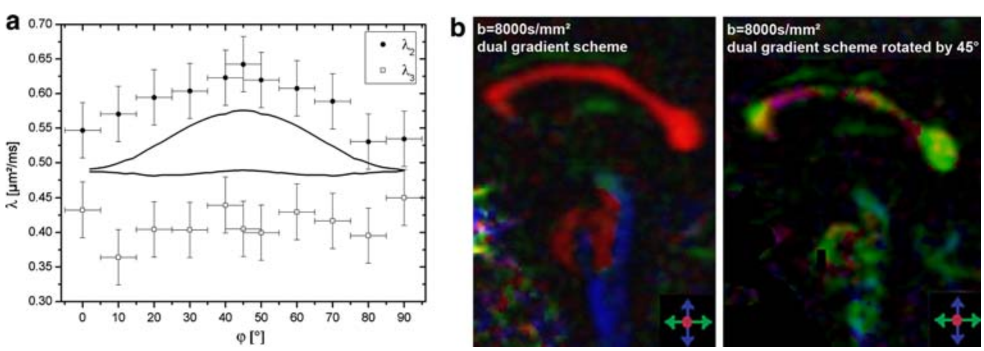

Fig. 5 **a** Secondary and tertiary eigenvalues in the Corpus Callosum measured with the 6-direction gradient scheme. φ represents the rotational angle of the gradient scheme along the head-feed axis. The tertiary eigenvalue is clearly orientation dependent due to the background noise. **b** Colormap of the corpus callosum and the medulla oblongata, acquired with a large b value of 8,000 s/mm^2. For the dual gradient scheme, the main fiber directions are represented correctly. If the gradient scheme is rotated by 45°, the principal eigenvectors wrongly point in the anterior–posterior direction since the eigenvalues are misordered

In vivo data

Figure 5a shows secondary and tertiary eigenvalues of the corpus callosum that were measured using the clinical parameter setting(i). Here, φ is the angle that the gradient scheme was rotated around the head-feed axis. The secondary eigenvalue is clearly dependent on the orientation of the gradient scheme and becomes largest for $\varphi = 45°$. The solid line represents theoretically computed values for a cigar shaped tensor with FA = 0.7, ADC = 1 µm^2/ms and SNR = 10. The shape of the solid line corresponds qualitatively and quantitatively to the measured values. The difference of secondary and tertiary eigenvalue for $\varphi = 0°$ can be attributed to the eigenvalue sorting bias [18].

Figure 5b shows colormaps covering the corpus callosum and the medulla oblongata, acquired with a large b value of 8,000 s/mm^2. For the dual gradient scheme, the main fiber directions are represented correctly, but if the gradient scheme is rotated by 45°, the principal eigenvectors of corpus callosum and medulla oblongata incorrectly point in the anterior–posterior direction since the eigenvalues are misordered. In the central part of the Corpus Callosum, the misordering is not observed since the FA is smaller than in the outer part [19].

Discussion

In this work, two novel background noise effects on DTI are presented. The underestimation of diffusion in the presence of background noise can cause both, an misordering of eigenvalues and a systematic eigenvector shift. The uncertainty of eigenvector direction was previously described by the cone of uncertainty [20] and in a later work, an orientation dependency of the cone of uncertainty was recognized [14]. Here, we show that besides this uncertainty, also the mean eigenvector direction is systematically shifted.

Both effects are important when condition (1) is violated, which may be the case in variety of settings. In high resolution applications, like DTI of the spinal cord [21] or optic nerve [22], the SNR is inherently small, such that background noise effects can be relevant even for moderate b values. For large b values, they can still be relevant, even if high SNRs are achieved in unweighted images. Large b values are applied, e.g. for the detection of water compartmentation [23,24] or for functional DWI [17]. Measurements can also be strongly affected if ADC or FA increase unexpectedly under pathological conditions [19]. Then, eigenvectors may be shifted unnoticed.

Note that Eq. (1) can be violated using parameters that are well within the current standard setting of DTI, like the in vivo parameter set (i) [25]. The increasing secondary eigenvalue can falsify image contrast based on eigenvalues [26] and the biased eigenvalues and the consequent erroneous FA can be misinterpreted as changes in fiber integrity due to pathological processes such as infiltration [19]. This especially hampers quantitative evaluations and has to be allowed for.

The data presented here (Figs. 2, 3, 5) was acquired using very high b values to amplify the presented effects. In practical applications, the errors may be smaller but still present. Moreover, subtle eigenvector shifts are hardly visible on colormaps since the color encoding is usually very sparse. Moreover, the main white matter tracts, such as the corpus callosum, the spinal cord, the cortico-spinal tract and the optic nerve, which can serve as orientational landmarks, run along 'attractive' orientations using the dual gradient scheme and appear in the correct color. Here, very high b value images may be acquired without necessarily noticing the eigenvector shift or the eigenvalue overestimation. Since the scatter of the data is reduced at large b values, the data may even appear to be more precise. Especially fiber tracking algorithms suffer from the observed systematic eigenvector shift, since systematic tracking errors add up much faster than random errors.

There are several strategies to circumvent background noise effects. The most obvious approach is to work with very high SNR images only. However, SNR is usually very limited in in vivo diffusion measurements if reasonable resolutions are required. Technical advances like higher field strengths, better coil design etc. may improve SNR, but are either expensive or technically challenging. Noise corrections as proposed by Gudbjartsson [2], Dietrich et al. [27], Wirestam et al. [28] or Wood et al. [29] may reduce the bias to a certain degree, but cannot completely solve the problem since the signal decays exponentially. If more than six gradient directions are acquired, gradient directions with insufficient signal may be omitted at the cost of time efficiency. Another possible solution is the acquisition of a series of b values and to fit the signal curve with an estimator of the noise. This was successfully applied by Jones et al. [3], but requires longer measurement times. Another promising approach, the application of Rician noise models for the estimation of the diffusion tensor, was successfully applied by Anderson et al. [30]. All these approaches to circumvent the signal bias can reduce or even mainly solve the signal bias. However, few of these strategies are commonly employed, thus our findings are of relevance for current clinical studies that employ DTI. Furthermore, even if post processing correction schemes are employed, the limits of the correction scheme must be considered carefully.

Since both artefacts presented in this paper are orientation dependent, they can be suppressed by using at least 20 gradient directions (Fig. 4) [14]. However, it is important to bear in mind that FA and ADC are still biased, while only the orientational variation is reduced [25].

In conclusion, two novel background noise effects on DTI were presented, a systematic eigenvector shift and the overestimation of certain eigenvalues. Both effects were observed in phantom and in vivo measurements following current standards and were described analytically.

Acknowledgment We thank Sarah Snyder for helpful discussions.

References

1. Henkelman RM (1985) Measurement of signal intensities in the presence of noise in MR images. Med Phys 12:232–233

2. Gudbjartsson H, Patz S (1995) The Rician distribution of noisy MRI data. Magn Reson Med 34:910–914
3. Jones DK, Basser PJ (2004) Squashing peanuts and smashing pumpkins: how noise distorts diffusion-weighted MR data. Magn Reson Med 52:979–993
4. Skare S, Hedehus M, Moseley ME, Li TQ (2000) Condition number as a measure of noise performance of diffusion tensor data acquisition schemes with MRI. J Magn Reson 147:340–352
5. Skare S, Li T, Nordell B, Ingvar M (2000) Noise considerations in the determination of diffusion tensor anisotropy. Magn Reson Imaging 18:659–669
6. Hasan KM, Parker DL, Alexander AL (2001) Comparison of gradient encoding schemes for diffusion-tensor MRI. J Magn Reson Imaging 13:769–780
7. Batchelor PG, Atkinson D, Hill DL, Calamante F, Connelly A (2003) Anisotropic noise propagation in diffusion tensor MRI sampling schemes. Magn Reson Med 49:1143–1151
8. Anderson AW (2001) Theoretical analysis of the effects of noise on diffusion tensor imaging. Magn Reson Med 46:1174–1188
9. Koay CG, Chang LC, Pierpaoli C, Basser PJ (2007) Error propagation framework for diffusion tensor imaging via diffusion tensor representations. IEEE Trans Med Imaging 26:1017–1034
10. Koay CG, Chang LC, Carew JD, Pierpaoli C, Basser PJ (2006) A unifying theoretical and algorithmic framework for least squares methods of estimation in diffusion tensor imaging. J Magn Reson 182:115–125
11. Koay CG, Carew JD, Alexander AL, Basser PJ, Meyerand ME (2006) Investigation of anomalous estimates of tensor-derived quantities in diffusion tensor imaging. Magn Reson Med 55: 930–936
12. Koay CG, Nevo U, Chang LC, Pierpaoli C, Basser PJ (2008) The elliptical cone of uncertainty and its normalized measures in diffusion tensor imaging. IEEE Trans Med Imaging 27:834–846
13. Chang LC, Koay CG, Pierpaoli C, Basser PJ (2007) Variance of estimated DTI-derived parameters via first-order perturbation methods. Magn Reson Med 57:141–149
14. Jones DK (2004) The effect of gradient sampling schemes on measures derived from diffusion tensor MRI: a Monte Carlo study. Magn Reson Med 51:807–815
15. Laun FB, Stieltjes B, Huff S, Schad LR (2007) Investigations of a DTI—phantom with properties similar to in vivo neuronal tissue. In: Proceedings of the ISMRM. Berlin, p 1526
16. Laun FB, Huff S, Stieltjes B (2008) On the effects of dephasing due to local gradients in diffusion tensor imaging experiments: relevance for diffusion tensor imaging fiber phantoms. Magn Reson Imaging. doi:10.1016/j.mri.2008.08.011 (accepted)
17. Jones DK, Horsfield MA, Simmons A (1999) Optimal strategies for measuring diffusion in anisotropic systems by magnetic resonance imaging. Magn Reson Med 42:515–525
18. Basser PJ, Pajevic S (2000) Statistical artifacts in diffusion tensor MRI (DT-MRI) caused by background noise. Magn Reson Med 44:41–50
19. Stieltjes B, Schluter M, Didinger B, Weber MA, Hahn HK, Parzer P, Rexilius J, Konrad-Verse O, Peitgen HO, Essig M (2006) Diffusion tensor imaging in primary brain tumors: reproducible quantitative analysis of corpus callosum infiltration and contralateral involvement using a probabilistic mixture model. Neuroimage 31:531–542
20. Jones DK (2003) Determining and visualizing uncertainty in estimates of fiber orientation from diffusion tensor MRI. Magn Reson Med 49:7–12
21. Bammer R, Fazekas F (2003) Diffusion imaging of the human spinal cord and the vertebral column. Top Magn Reson Imaging 14:461–476
22. Wheeler-Kingshott CA, Trip SA, Symms MR, Parker GJ, Barker GJ, Miller DH (2006) In vivo diffusion tensor imaging of the human optic nerve: pilot study in normal controls. Magn Reson Med 56:446–451
23. Clark CA, Le Bihan D (2000) Water diffusion compartmentation and anisotropy at high *b* values in the human brain. Magn Reson Med 44:852–859
24. Maier SE, Vajapeyam S, Mamata H, Westin CF, Jolesz FA, Mulkern RV (2004) Biexponential diffusion tensor analysis of human brain diffusion data. Magn Reson Med 51:321–330
25. Laun FB, Stieltjes B, Schad LR (2007) Influence of the noise floor: paradoxical effects on DTI. In: Proceedings of the ISMRM. Berlin, p 1594
26. Zhang J, van Zijl PC, Mori S (2006) Image contrast using the secondary and tertiary eigenvectors in diffusion tensor imaging. Magn Reson Med 55:439–449
27. Dietrich O, Heiland S, Sartor K (2001) Noise correction for the exact determination of apparent diffusion coefficients at low SNR. Magn Reson Med 45:448–453
28. Wirestam R, Bibic A, Lätt J, Brockstedt S, Ståhlberg F (2006) Denoising of complex MRI data by wavelet-domain filtering: application to high-b-value diffusion-weighted imaging. Magn Reson Med 56:1114–1120
29. Wood JC, Johnson KM (1999) Wavelet packet denoising of magnetic resonance images: importance of Rician noise at low SNR. Magn Reson Med 41:631–635
30. Andersson JL (2008) Maximum a posteriori estimation of diffusion tensor parameters using a Rician noise model: why, how and but. Neuroimage 42(4):1340–1356